Journal of Materials Chemistry B

ROYAL SOCIETY OF CHEMISTRY

PAPER

View Article Online
View Journal | View Issue

Check for updates

Cite this: J. Mater. Chem. B, 2026, 14, 4311

Water-soluble acylhydrazone macrocycles as potent reversal agents for cisatracurium-induced neuromuscular blockade

Yongfei Yin,†[c] Yangyang Ge,†[b] Qian Li,†[a] Yi Chen,[a] Siyuan Zhou,[a] He Deng,[a] Shigui Chen,*[a] Yun Lin*[b] and Lu Wang*[a]

Received 20th December 2025, Accepted 7th March 2026

DOI: 10.1039/d5tb02867a

rsc.li/materials-b

Cisatracurium is a widely used non-depolarizing neuromuscular blocking agent during anesthesia; however, residual neuromuscular blockade post-surgery can lead to severe respiratory complications, highlighting the urgent need for effective reversal agents. In this study, we designed and synthesized a highly water-soluble acylhydrazone macrocycle featuring an electron-rich cavity as an efficient supramolecular reversal agent for cisatracurium. The macrocycle binds cisatracurium through electrostatic and hydrophobic interactions, exhibiting a binding constant of up to 10^5 M^{-1}. Cytotoxicity assays confirmed its excellent biocompatibility, and *in vivo* studies in cisatracurium-anesthetized mice demonstrated that the macrocycle effectively reverses cisatracurium-induced neuromuscular blockade. This work provides a new strategy for developing water-soluble acylhydrazone macrocycles as potential supramolecular reversal agents for neuromuscular blockers.

Introduction

In clinical anesthesia practice, neuromuscular blocking agents (NMBAs) are among the most frequently administered drugs prior to surgery.[1] Intravenous administration of NMBAs induces skeletal muscle relaxation by blocking neuromuscular transmission, thereby reducing muscle reflex-related interference during surgical manipulation, improving operative conditions, facilitating tracheal intubation, and providing better visualization for procedures involving the thoracic or abdominal cavities. Rapid and complete reversal of neuromuscular block at the end of surgery is essential for the timely recovery of spontaneous respiration and for reducing the risk of residual neuromuscular block (RNMB), making it a critical component of anesthetic management.[2]

Traditional reversal agents are primarily acetylcholinesterase inhibitors, such as neostigmine and edrophonium.[3–5] These agents inhibit the breakdown of acetylcholine, increasing its concentration at the neuromuscular junction and enhancing its ability to outcompete NMBAs for binding to nicotinic acetylcholine receptors (nAChRs), thereby reversing neuromuscular block. However, their reversal efficacy is limited, and they are often associated with adverse effects including bradycardia and bronchospasm.[6] In recent years, with the rapid progress of supramolecular chemistry,[7–10] "supramolecular reversal agents" based on host–guest interactions have emerged as a promising strategy for NMBA reversal.[11–14] Macrocyclic hosts such as cyclodextrins, pillararenes,[15–21] cucurbiturils,[22–26] and calixarenes[27,28] have been explored for the design of agents capable of selectively binding and clearing NMBAs. Among them, the γ-cyclodextrin derivative Sugammadex represents a major clinical breakthrough,[29] efficiently reversing aminosteroid NMBAs such as rocuronium (Roc), vecuronium (Vec), and pancuronium (Pan) through inclusion complexation. Nevertheless, the cavity size of cyclodextrins limits their ability to encapsulate bulkier neuromuscular blockers. As a result, Sugammadex shows poor efficacy against larger and more rigid NMBAs such as cisatracurium (**Cis**) and other benzylisoquinolinium compounds.[30] Notably, **Cis** is widely used in intensive care units and is considered the NMBA of choice for patients at high risk of acute respiratory distress syndrome (ARDS), due to its organ-independent metabolism and minimal histamine release.[31] Therefore, there is an urgent clinical need for a supramolecular antagonist capable of rapidly and efficiently reversing **Cis**-induced neuromuscular block.

Hydrogen-bonded aromatic amide/hydrazone macrocycles constitute an emerging class of cyclic compounds constructed

[a] The Institute for Advanced Studies, Hubei Key Lab on Organic and Polymeric Opto-Electronic Materials, Wuhan University, 299 Bayi Road, Wuhan, Hubei 430072, China. E-mail: sgchen@whu.edu.cn, wanglu-027@whu.edu.cn
[b] Department of Anesthesiology, Union Hospital, Tongji Medical College, Huazhong University of Science and Technology, Jiefang Road 1277, Wuhan, Hubei 430022, China. E-mail: franklinyun@hust.edu.cn
[c] Biomass Oligosaccharides Engineering Technology Research Center of Anhui Province, School of Chemistry and Material Engineering, Fuyang Normal University, 100 Qinghe West Road, Fuyang, Anhui 236000, China
† Equally contributed to this work.

from consecutive intramolecular hydrogen bonds and aromatic units.[32–34] Owing to their high conformational rigidity, tunable structural features, readily functionalizable molecular frameworks, electron-rich cavities, and versatile host–guest recognition capabilities, these macrocycles have been extensively explored and applied in diverse research areas, including supramolecular vesicles,[35] artificial ion channels,[36,37] gels,[38–40] supramolecular catalysis,[41–43] and artificial molecular machines.[44] Importantly, these properties also suggest the potential of aromatic amide/hydrazone macrocycles as supramolecular antagonists for NMBAs, yet, to the best of our knowledge, no such application has been reported to date.

Herein, we report the design and synthesis of a water-soluble hydrazone-based macrocyclic compound, **PEG-MC**, featuring a large electron-rich cavity and a rigid framework. The compound selectively binds the bulky **Cis** molecule *via* host–guest recognition, exhibiting a high binding constant of 5.58×10^5 M^{-1} in aqueous solution. *In vivo*, **PEG-MC** markedly accelerates recovery from **Cis**-induced neuromuscular blockade (NMB), shortening the time to spontaneous respiration from 78.8 s to 51.5 s. These results establish **PEG-MC** as a highly effective supramolecular antagonist and exemplify the potential of rational macrocyclic design for developing next-generation reversal agents for neuromuscular blockers (Scheme 1).

Experimental section

Cell culture

293 T cells were incubated in complete culture medium comprising DMEM supplemented with 10% FBS, 100 IU mL^{-1} penicillin, and 100 mg mL^{-1} streptomycin, and then cultured at 37 °C in a humidified atmosphere with 5% CO_2. The attached cells were routinely passaged with a 0.25% trypsin-EDTA solution after reaching 80% confluency. The medium was replaced every 3 days.

Cytotoxicity experiments

To evaluate the cytotoxicity of **PEG-MC**, an MTT cell proliferation and cytotoxicity assay kit (Beyotime Biotechnology) was used for toxicity studies. Following cell digestion and counting, 5000 cells per well were seeded in a 96-well plate. After a 2-day culture period, **PEG-MC** was added to six wells designated for each drug concentration. Following a 24 h incubation period, 10 μL of MTT solution (0.5 mg mL^{-1}) was added to each well for a 4 h incubation. Subsequently, 100 μL of formazan solution was added to dissolve the dark blue formazan crystals. The absorbance was measured at 570 nm using a microplate reader. The cell viability rate is presented as a percentage ratio between the absorbance of the treated group and that of the control group.

Respiratory monitoring

C57BL/6 mice (8 weeks old; body weight 24.0–26.0 g) were used in this study. All drugs were administered *via* tail vein injection. The animals were randomly assigned to two groups: (1) the **Cis** group, in which **Cis** was prepared as an aqueous solution at a concentration of 1.0 mg mL^{-1} and administered at an injection volume of 1 mL; and (2) the **Cis** + **PEG-MC** premix group, in which **PEG-MC** was fully dissolved in the **Cis** aqueous solution to obtain a formulation containing 1.0 mg mL^{-1} **Cis** and 2.13 mg mL^{-1} **PEG-MC**, with an injection volume of 1 mL. All formulations were

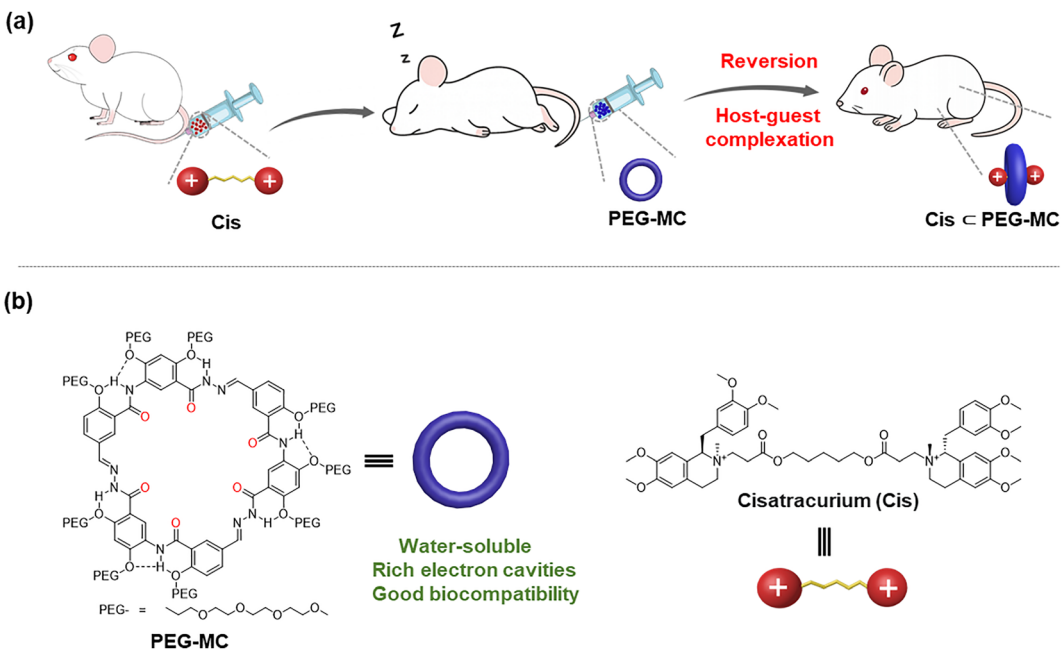

Scheme 1 (a) Schematic illustration of the host–guest encapsulation strategy based on water-soluble hydrazone-based macrocyclic **PEG-MC** to reverse the NMB effect of cisatracurium **Cis**. (b) Chemical structures of **PEG-MC** and **Cis**.

stored at 4 °C prior to use. The entire experimental procedure was video-recorded to enable continuous monitoring of diaphragmatic movements. The time interval between the cessation of diaphragmatic movement and the first observable reappearance of movement was measured and defined as the spontaneous breathing recovery time (s). Animals were excluded from the analysis if drug extravasation or injection failure occurred during tail vein administration. All animals received care in compliance with the guidelines outlined in the Guide for the Care and Use of Laboratory Animals. All of the animal experiments were approved by the Institutional Animal Care and Use Committee of Huazhong University of Science and Technology ([2023] IACUC Number: 4887).

Statistical analysis

The experimental data were expressed as mean ± standard error (mean ± SEM) using GraphPad and Origin SPSS software was used for statistical analysis. Comparison between the two groups was performed using a paired *t*-test, and $P < 0.05$ was considered statistically significant (****: $P < 0.0001$; ***: $P < 0.001$; **: $P < 0.01$; and *: $P < 0.05$).

Results and discussion

Host–guest interactions between Cis and C8-MC

To verify the potential of the acylhydrazone macrocycle as a supramolecular antagonist for cis-atracurium **Cis**, a lipophilic acylhydrazone macrocycle bearing an octyl chain (**C8-MC**) was designed and synthesized. First, the host–guest interactions between **C8-MC** and **Cis** in the organic phase were investigated by ^{1}H NMR titration experiments in a $CDCl_3$/DMSO-d_6 (4 : 1, *v*/*v*) solvent system (Fig. 1a and Fig. S1). The results showed that with the gradual increase of the **Cis** concentration, significant changes in both the peak shape and chemical shift were observed for the characteristic proton signals of **C8-MC** and **Cis**, indicating the occurrence of distinct host–guest interactions between them. Furthermore, the chemical shift variations ($\Delta\delta = \delta_{obsd} - \delta_{free}$) of the characteristic protons in **Cis** were analyzed after mixing **C8-MC** and **Cis** at a 1 : 1 molar ratio (Fig. 1b). It was found that the signals of H_a and H_c protons on the quaternary ammonium head group of **Cis** shifted downfield due to deshielding effects, while the signals of H_d, H_e, and H_f protons on the alkyl chain shifted upfield because of shielding effects. These observations suggest that the H_a and H_c protons

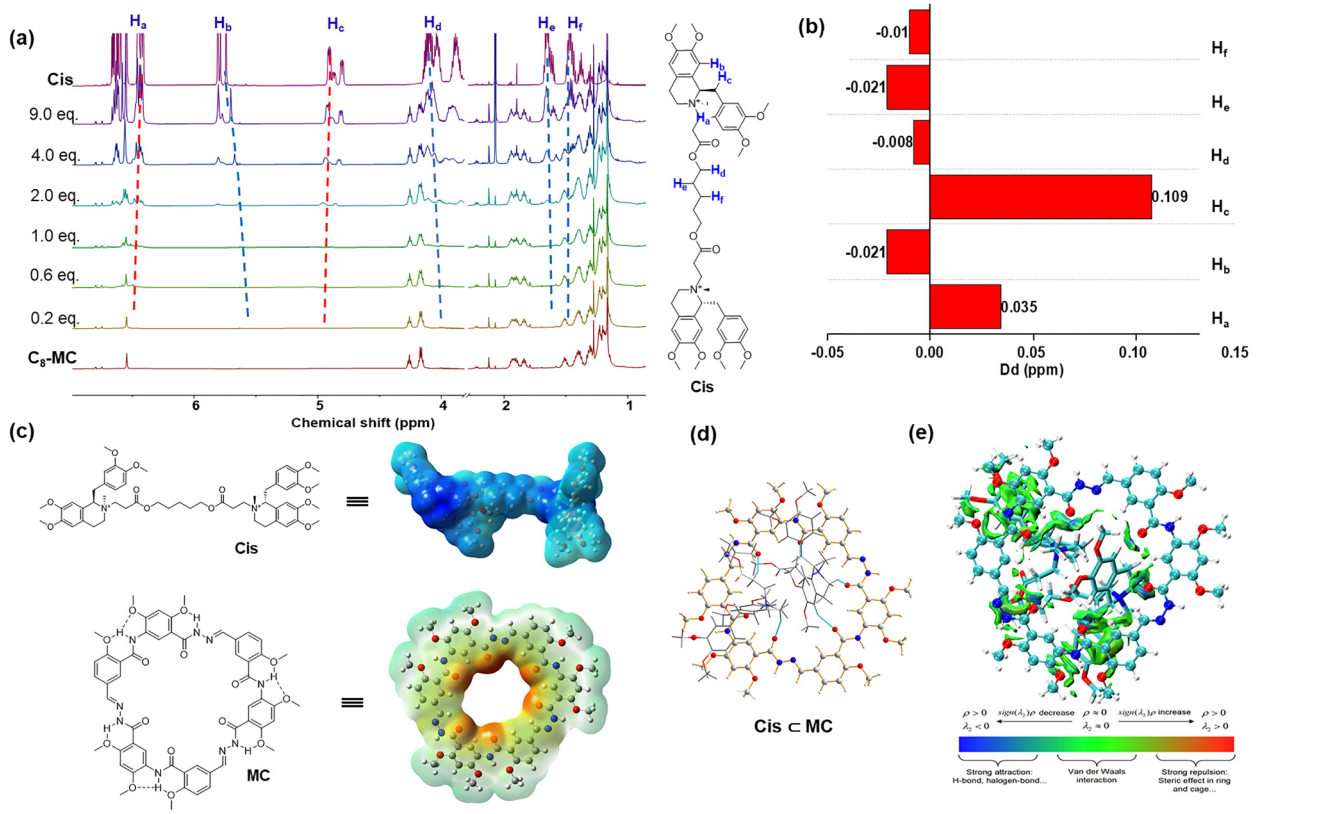

Fig. 1 (a) Partial ^{1}H NMR spectra (600 MHz, 298 K) of **C8-MC** (1.00 mM in $CDCl_3$: DMSO-d_6 = 4 : 1, v/v) upon incremental addition of **Cis** (0–9 equiv.). (b) Normalized ^{1}H NMR chemical shift changes ($\Delta\delta = \delta_{obsd} - \delta_{bound}$) of **Cis** protons as a function of the guest concentration titrated into a 1.00 mM solution of **C8-MC** ($CDCl_3$: DMSO-d_6 = 4 : 1, v/v). (c) Molecular electrostatic potential (ESP) surfaces of **C8-MC** and **NMBA**. (d) Side view of the energy-minimized structure of the **Cis**⊂**MC** complex. (e) Top-down view of the noncovalent interaction surfaces of complex **Cis**⊂**MC**. $\Delta\kappa_{inter(\rho)} = 0.005$ a.u. Isosurfaces are colored according to the blue-green-red (BGR) scheme over the range $-0.03 < \mathrm{sign}(\lambda_2)\rho < +0.05$ a.u. The scale bar represents the color mapping for noncovalent interaction surfaces derived from IGM analysis.

of **Cis** are located deep inside the cavity of **C8-MC**, whereas H_d, H_e, and H_f are positioned near the rim of the cavity. In addition, the continuous variation method (Job's plot) confirmed a 1 : 1 binding stoichiometry between **C8-MC** and **Cis**. The association constant (K_a) was determined to be $4.40 \times 10^3\ M^{-1}$ by nonlinear curve fitting (Fig. S2).

Density functional theory (DFT) calculations were performed to provide deeper insight into the host–guest interactions and the binding mechanism between **C8-MC** and **Cis** by analyzing the structural characteristics of the complex. To simplify the computational model, a macrocycle with an identical framework (**MC**) was employed as a representative analog of **C8-MC** (Fig. 1c). The optimized geometry revealed that the originally symmetric structure of **Cis** became significantly

distorted upon complexation and penetrated through the cavity of **MC** (Fig. 1d and Fig. S3), indicating a pronounced host–guest interaction. Moreover, the H_a and H_c protons of **Cis** were located deep within the cavity of **MC**, which is consistent with the results obtained from the ^{1}H NMR titration experiments. Further electronic structure analysis was conducted by calculating the highest occupied molecular orbital (HOMO), lowest unoccupied molecular orbital (LUMO) (Fig. S4), and electrostatic potential (ESP) distributions of the **MC**⊃**Cis** complex (Fig. S5). The ESP mapping showed that the cavity of **MC** possessed a strongly negative potential, whereas the quaternary ammonium head of **Cis** exhibited an evident positive potential. This electrostatic complementarity facilitates the formation of a stable complex through ion–dipole and other noncovalent interactions. In addition, both the HOMO and LUMO distributions of the host and guest molecules exhibited noticeable changes after complexation, further suggesting electronic interactions between them.

To visualize the noncovalent interactions (NCIs) between **MC** and **Cis**, Multiwfn and VMD software were employed, and the interaction patterns were analyzed using the independent gradient model (IGM) approach. The resulting NCI plots clearly illustrated multiple ion–dipole interactions between **MC** and **Cis** (Fig. 1e), confirming that the host–guest interaction is primarily driven by ion–dipole and other noncovalent forces.

Host–guest interactions between Cis and PEG-MC

Acylhydrazone macrocycles (MC) were demonstrated to accommodate the relatively large anesthetic molecule **Cis**. To further improve the water solubility of the aromatic acylhydrazone macrocycle and enable its application in more complex biological systems, nine polyethylene glycol (PEG) chains were introduced onto the macrocyclic backbone, leading to the successful synthesis of the water-soluble PEG-functionalized acylhydrazone macrocycle (**PEG-MC**) (Scheme 2).

Subsequently, the host–guest interactions between **PEG-MC** and **Cis** in aqueous solution were investigated using ^{1}H NMR spectroscopy. Due to pronounced aggregation of **PEG-MC** in water, the ^{1}H NMR spectrum of the macrocycle was complex, and the assignment of its protons was challenging (Fig. S6). Nevertheless, upon gradual addition of **Cis** to a D_2O solution of **PEG-MC**, significant changes were observed in the characteristic proton signals of **Cis** (Fig. S7). Normalized chemical shift changes ($\Delta\delta = \delta_{obsd} - \delta_{bound}$) were plotted to analyze the proton

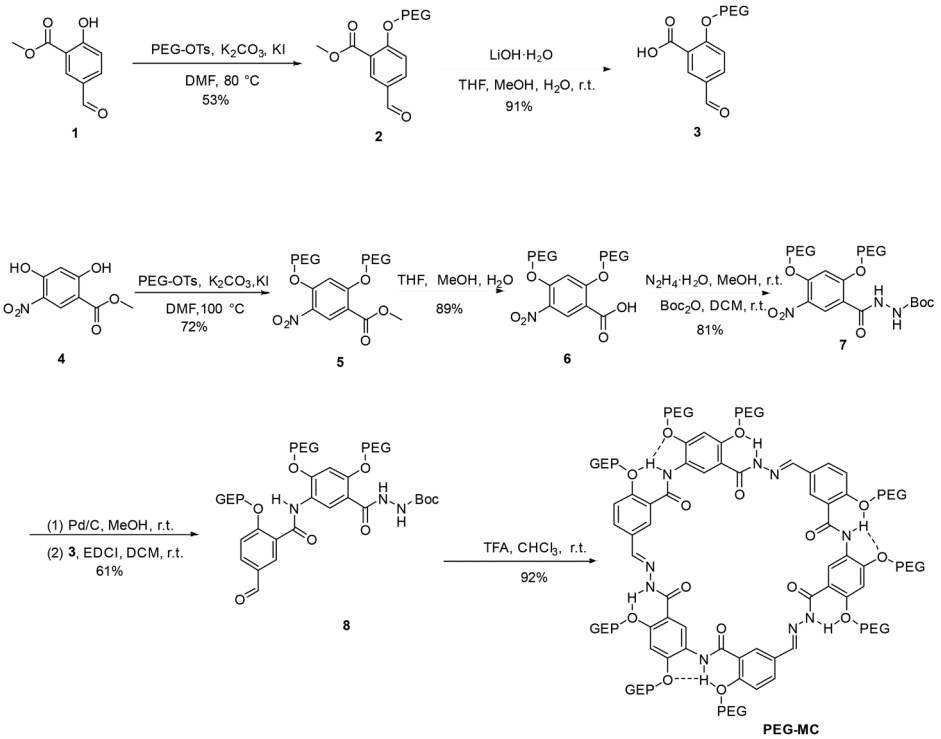

Scheme 2 Synthesis route to **PEG-MC**.

shift trends of **Cis** as its concentration increased in the **PEG-MC** solution (Fig. S8). The results revealed that the chemical shifts of the protons on the alkyl chain of **Cis** (H_d, H_e, H_f) changed most significantly ($\Delta\delta$ = −0.025, −0.106, −0.052 ppm), whereas the aromatic proton H_a exhibited a minimal shift ($\Delta\delta$ = −0.003 ppm). Notably, the pronounced shift of H_e suggests that the alkyl chain of **Cis** is deeply embedded within the electron-rich cavity of **PEG-MC**, while the aromatic ring remains positioned near the cavity periphery.

The host–guest interactions and assembly mechanism of **PEG-MC** with **Cis** in aqueous solution were similarly examined through DFT calculations and structural optimizations. To simplify the computational model, **MC** was used as a representative. The optimized structure of the **MC**⊃**Cis** complex revealed that the macrocyclic backbone of **MC** exhibits slight bending and is positioned near the quaternary ammonium head of **Cis** (Fig. S9), indicating a pronounced host–guest interaction. Notably, the H_e proton of **Cis** is located deep within the cavity of **MC**, whereas the H_a proton resides near the cavity periphery, consistent with the previously obtained ^{1}H NMR titration results.

Further electronic structure analysis was conducted by examining the HOMO, LUMO, and ESP distributions. In the free state, the HOMO and LUMO of **MC** are mainly localized on the benzene rings of the macrocyclic backbone, while those of **Cis** are concentrated on its aromatic head. Upon complexation, significant changes in both the HOMO and LUMO distributions were observed (Fig. S10), further confirming electronic interactions between the host and guest. The ESP mapping showed that the cavity of **MC** is strongly negative, whereas the quaternary ammonium head of **Cis** exhibits pronounced positive potential (Fig. S11), facilitating stable complex formation through electrostatic and other noncovalent interactions. Additionally, charge transfer from **Cis** to **MC** results in an increase in local positive charge density on **MC**, suggesting the presence of cation–π interactions. Finally, noncovalent interaction (NCI) analysis revealed that in aqueous solution (Fig. S12), **Cis** penetrates the cavity of **MC**, and multiple noncovalent interactions exist between the quaternary ammonium head of **Cis** and the macrocyclic backbone of **MC**, leading to the formation of a stable 1 : 1 host–guest complex. Overall, the host–guest association between **MC** and **Cis** is primarily driven by cation–π and hydrophobic interactions.

The host–guest interactions between **PEG-MC** and **Cis** in aqueous solution were further investigated using UV-visible spectroscopy (UV-vis) and isothermal titration calorimetry (ITC) experiments. As shown in Fig. 2a, upon gradual addition of **Cis** to the **PEG-MC** aqueous solution, the characteristic absorption band of the acylhydrazone macrocycle at 315 nm decreased markedly in intensity. A distinct inflection point was observed at 1.0 equivalent of **Cis** (Fig. 2b), indicating a 1 : 1 host–guest stoichiometry between **PEG-MC** and **Cis**. Nonlinear least-squares fitting afforded an association constant (K_a) of 5.98 × 10^5 M^{-1} (Fig. S13). Consistently, ITC measurements confirmed the 1 : 1 complexation between **PEG-MC** and **Cis**, with a binding constant of 5.58 × 10^5 M^{-1}, in good agreement with the UV–vis titration results. The corresponding thermodynamic parameters were determined as ΔG = −7.87 kcal mol^{-1}, ΔH = −0.530 kcal mol^{-1}, and ΔS = −2.46 × 10^{-2} kcal mol^{-1} K^{-1}. These results suggest that the formation of the **Cis**⊂**PEG-MC** complex is primarily enthalpy-driven and exhibits high binding stability. Moreover, the pronounced exothermic peaks observed in the ITC thermograms imply that a certain degree of aggregation occurs during the complexation process.[45] To verify this hypothesis, the self-assembly behavior of **Cis**⊂**PEG-MC** was further characterized by dynamic light scattering (DLS) and transmission electron microscopy (TEM). DLS analysis revealed that **PEG-MC** alone exhibited a hydrodynamic diameter (D_h) centered at approximately 531 nm with a polydispersity index (PDI) of 0.2, whereas the addition of an equimolar amount of **Cis** increased D_h to about 955 nm with a PDI of 0.4 (Fig. S15). To further evaluate the stability of **PEG-MC** in aqueous media, its particle size distribution was monitored over time. After storage at room temperature for 10 days, the D_h of **PEG-MC** increased slightly to approximately 610 nm, with a PDI of

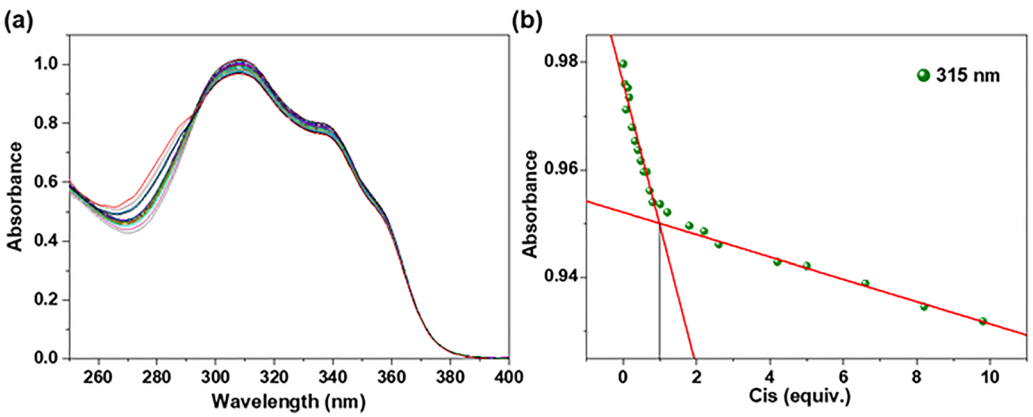

Fig. 2 (a) UV-vis absorption spectra of the mixture of **PEG-MC** and **Cis** in aqueous solution at different molar ratios. (b) Plot showing the 1 : 1 stoichiometry of the complex between **PEG-MC** and **Cis** by plotting the difference in absorption at 315 nm (a characteristic absorption peak of **PEG-MC**) against the molar fraction of **Cis** at an invariant total concentration of 0.033 mM in aqueous solution.

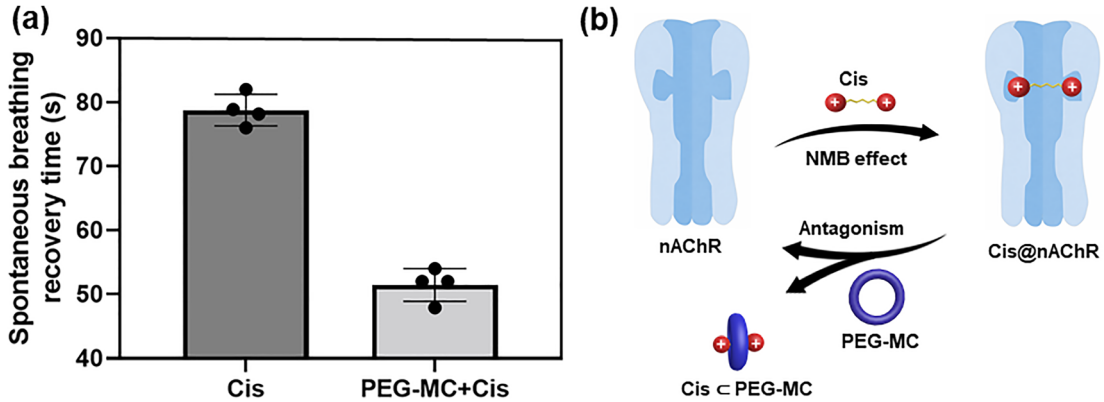

Fig. 3 (a) Results of the *in vivo* efficacy studies conducted using Sprague-Dawley rats. Rats (n = 4 per group) were anesthetized with isoflurane and treated with a neuromuscular blocker **Cis** and then treated with saline or **PEG-MC**. Error bars represent means and standard deviation, *$p < 0.05$; **$p < 0.01$; ***$p < 0.001$; and ****$p < 0.0001$ (unpaired two-tailed t-test). (b) Schematic illustration of using **PEG-MC** as a selective relaxant binding agent against the neuromuscular blocking agent.

0.38 (Fig. S16). Although small increases in particle size and dispersity were observed, no significant large-scale aggregation or precipitation occurred, indicating that the system exhibits good stability. TEM images showed that **PEG-MC** self-assembled into spherical nanoparticles with an average diameter of ~451 nm, while **Cis⊂PEG-MC** formed larger spherical nanoparticles with an average diameter of ~1106 nm (Fig. S17). Taken together, these findings demonstrate that the host–guest interactions between **Cis** and **PEG-MC** significantly promote further aggregation and hierarchical self-assembly of **PEG-MC**, leading to the formation of larger supramolecular nanoparticles in aqueous solution.

Experiment for reversal of Cis *in vivo*

Given the strong binding affinity of **PEG-MC** toward **Cis**, we further investigated its ability to reverse neuromuscular blockade *in vivo*. Prior to the animal studies, the cytotoxicity of **PEG-MC** was assessed using the MTT assay in human embryonic kidney 293T cells. The results showed that **PEG-MC** exhibited negligible cytotoxicity, likely owing to the presence of eight hydrophilic PEG chains. Even at a relatively high concentration of 80 μM, the cell viability remained above 80% (Fig. S18), indicating that **PEG-MC** possesses good biocompatibility.

Subsequently, rats (n = 4) were anesthetized with isoflurane and tracheally intubated for mechanical ventilation and respiratory monitoring to assess the neuromuscular blockade reversal effect of **PEG-MC**. The results showed that the recovery time of spontaneous respiration in the control group was 78.8 seconds, while intravenous injection of **PEG-MC** significantly reduced the recovery time to 51.5 seconds (Fig. 3a). These results indicate that **PEG-MC** can strongly bind free **Cis** molecules *in vivo*, thereby competing with the binding sites of nAChRs on the postsynaptic membrane and effectively reversing the neuromuscular transmission blockade caused by **Cis** (Fig. 3b). **PEG-MC** reduces the effective concentration of **Cis** in the body, thereby weakening or even eliminating its inhibitory effect on synaptic transmission and promoting the rapid recovery of spontaneous respiration in anesthetized animals. In summary, **PEG-MC** exhibited excellent biocompatibility and remarkable *in vivo* efficacy in reversing **Cis**-induced neuromuscular blockade, demonstrating its potential as a supramolecular antidote for **Cis**.

Conclusions

In conclusion, we successfully synthesized the water-soluble hydrazone macrocycle **PEG-MC**. Detailed characterization demonstrated that **PEG-MC** forms a stable 1 : 1 pseudorotaxane-type complex with **Cis**, featuring a strong host–guest interaction with an association constant on the order of 10^5 M^{-1}. *In vitro* studies confirmed its excellent biocompatibility, and *in vivo* experiments further revealed that **PEG-MC** effectively reverses **Cis**-induced neuromuscular blockade in mice, shortening the recovery time of spontaneous respiration from 78.8 s to 51.5 s. Collectively, these findings validate **PEG-MC** as a promising candidate for clinically reversing **Cis** and highlight the broader potential of supramolecular therapeutic strategies in advancing biomedical interventions, particularly in anesthesia and the reversal of neuromuscular blockade.

Author contributions

Y. F. Yin: formal analysis, investigation, data curation, and writing of the original draft. Y. Y Ge: investigation and data curation. Q. Li: investigation, resources, and data curation. Y. Chen: compound synthesis, investigation, and data curation. S. Y. Zhou: compound synthesis, investigation, resources, and data curation. H. Deng: compound synthesis and investigation. S. G. Chen: conceptualization, writing – review and editing, supervision, project administration, and funding acquisition. Y. Lin: conceptualization, writing – review and editing, supervision, project administration, and funding acquisition. L. Wang: conceptualization, writing – review and editing, supervision, project administration, and funding acquisition.

Conflicts of interest

The authors declare no conflict of interest.

Data availability

All relevant data are within the manuscript and its supplementary information (SI). Supplementary information is available. See DOI: https://doi.org/10.1039/d5tb02867a.

Acknowledgements

This work was supported by the National Natural Science Foundation of China (22371218, 21702153, 52270070 and 21801194) and the Youth Program of Educational Commission of Anhui Province of China (2025AHGXZK40705). We thank the support of the Core Facility of Wuhan University and the Large-scale Instrument and Equipment Sharing Foundation of Wuhan University.

Notes and references

1 J. M. Hunter and M. Blobner, *Br. J. Anaesth.*, 2024, **132**, 461–465.
2 C. G. Stäuble and M. Blobner, *Curr. Opin. Anaesthesiol.*, 2020, **33**, 490–498.
3 N. J. Harper, E. G. Bradshaw and T. E. Healy, *Br. J. Anaesth.*, 1984, **56**, 1089–1094.
4 J. L. D. Thomsen, A. K. Staehr-Rye, O. Mathiesen, D. Hägi-Pedersen and M. R. Gätke, *Anaesthesia*, 2020, **75**, 1164–1172.
5 M. Sanfilippo, V. Vilardi, G. Fierro, G. Rosa, P. Pelaia and A. Gasparetto, *Acta Anaesthesiol. Scand.*, 1988, **32**, 437–440.
6 H.-C. Chang, S.-Y. Liu, M.-J. Lee, S.-O. Lee and C.-S. Wong, *J. Formosan Med. Assoc.*, 2022, **121**, 2639–2643.
7 D. B. Amabilino and P. A. Gale, *Chem. Soc. Rev.*, 2017, **46**, 2376–2377.
8 I. Alfonso, *Chem. Commun.*, 2024, **60**, 9692–9703.
9 A. A. H. Laporte and J. N. H. Reek, *Chem. Rev.*, 2025, **125**, 7223–7274.
10 C. Liu, Y. Jin, J. Li, Z. Wang, J. Wang and W. Tian, *Chin. J. Chem.*, 2025, **43**, 2053–2068.
11 Z. Wang, H. Yin and R. Wang, *J. Med. Chem.*, 2025, **68**, 6955–6957.
12 C.-L. Deng, S. L. Murkli and L. D. Isaacs, *Chem. Soc. Rev.*, 2020, **49**, 7516–7532.
13 J. M. Adam, D. J. Bennett, A. Bom, J. K. Clark, H. Feilden, E. J. Hutchinson, R. Palin, A. Prosser, D. C. Rees, G. M. Rosair, D. Stevenson, G. J. Tarver and M.-Q. Zhang, *J. Med. Chem.*, 2002, **45**, 1806–1816.
14 H. Yin, X. Zhang, J. Wei, S. Lu, D. Bardelang and R. Wang, *Theranostics*, 2021, **11**, 1513–1526.
15 W. Zhang, E. A. Bazan-Bergamino, A. P. Doan, X. Zhang and L. Isaacs, *Chem. Commun.*, 2024, **60**, 4350–4353.
16 Q. Zhao, J. Zhu, Y. Chen, H. Dong, S. Zhou, Y. Yin, Q. Cai, S. Chen, C. Chen and L. Wang, *J. Hazard. Mater.*, 2024, **469**, 133875.
17 Z. Fang, Z. Zhang, R. Wang, S. Li, S. Lin, Y. Zhou, J. Chen, C. Li and Q. Meng, *J. Med. Chem.*, 2024, **67**, 21568–21576.
18 X. Zhang, Q. Cheng, L. Li, L. Shangguan, C. Li, S. Li, F. Huang, J. Zhang and R. Wang, *Theranostics*, 2019, **9**, 3107–3121.
19 D. N. Shurpik, O. A. Mostovaya, D. A. Sevastyanov, O. A. Lenina, A. S. Sapunova, A. D. Voloshina, K. A. Petrov, I. V. Kovyazina, P. J. Cragg and I. I. Stoikov, *Org. Biomol. Chem.*, 2019, **17**, 9951–9959.
20 Y. Chai, L. Chen, Y. Zhang, L. Zhao, Z. Meng, J. Chen, C. Li and Q. Meng, *Chin. Chem. Lett.*, 2022, **33**, 3003–3006.
21 M. Li, Y. Cheng, R. Fei, D. Xia, Z. Zhang, S. Qi and J. Du, *Chem. Commun.*, 2025, **61**, 5982–5985.
22 D. Ma, B. Zhang, U. Hoffmann, M. G. Sundrup, M. Eikermann and L. Isaacs, *Angew. Chem., Int. Ed.*, 2012, **51**, 11358–11362.
23 J. Yang, Y. Wu, Y.-Y. Liu, S.-B. Yu, K. Feng, H. Wang, W. Zhou, D. Ma, G. Zhao, J. Zhang, D.-W. Zhang and Z.-T. Li, *J. Med. Chem.*, 2025, **68**, 7031–7043.
24 H.-K. Liu, F. Lin, S.-B. Yu, Y. Wu, S. Lu, Y.-Y. Liu, Q.-Y. Qi, J. Cao, W. Zhou, X. Li, H. Wang, D.-W. Zhang, Z.-T. Li and D. Ma, *J. Med. Chem.*, 2022, **65**, 16893–16901.
25 D. H. Macartney, *Future Med. Chem.*, 2013, **5**, 2075–2089.
26 Y. Wu, J. Yang, S.-Y. Zhuang, S.-B. Yu, Y. Zong, Y.-Y. Liu, G. Wu, Q.-Y. Qi, H. Wang, J. Tian, W. Zhou, D. Ma, D.-W. Zhang and Z.-T. Li, *J. Med. Chem.*, 2024, **67**, 2176–2187.
27 A. J. Selinger, N. A. Cavallin, A. Yanai, I. Birol and F. Hof, *Angew. Chem., Int. Ed.*, 2022, **61**, e202113235.
28 M. K. Abd El-Rahman and A. M. Mahmoud, *RSC Adv.*, 2015, **5**, 62469–62476.
29 A. Bom, M. Bradley, K. Cameron, J. K. Clark, J. van Egmond, H. Feilden, E. J. MacLean, A. W. Muir, R. Palin, D. C. Rees and M.-Q. Zhang, *Angew. Chem., Int. Ed.*, 2002, **41**, 265–270.
30 H. D. de Boer, J. van Egmond, F. van de Pol, A. Bom and L. H. Booij, *Br. J. Anaesth.*, 2006, **96**, 473–479.
31 V. C. Roy, S. Mehta and R. Bala, *Turk. J. Anaesthesiol. Reanim.*, 2025, **53**, 293–300.
32 Q. Li, H. Deng, W. Zeng, Q. Zhao, T. Zhan, S. Chen and L. Wang, *Chem. – Asian J.*, 2025, **20**, e202500289.
33 L.-L. Wang, Y.-K. Tu, A. Valkonen, K. Rissanen and W. Jiang, *Chin. J. Chem.*, 2019, **37**, 892–896.
34 W. Zeng, Q. Li, H. Deng, K.-D. Zhang, M. Zhang, Y. Yin, S. Chen and L. Wang, *Chin. Chem. Lett.*, 2026, DOI: 10.1016/j.cclet.2026.112526.
35 H. Deng, G. Gong, S. Lv, Y. Chen, Q. Zhao, S. Liu, S. Chen and L. Wang, *Org. Chem. Front.*, 2023, **10**, 317–326.
36 P. Saha and N. Madhavan, *Org. Lett.*, 2020, **22**, 5104–5108.
37 P. Xin, S. Tan, Y. Wang, Y. Sun, Y. Wang, Y. Xu and C.-P. Chen, *Chem. Commun.*, 2017, **53**, 625–628.
38 C. Ren, S. Xu, J. Xu, H. Chen and H. Zeng, *Org. Lett.*, 2011, **13**, 3840–3843.

39 Y. He, M. Xu, R. Gao, X. Li, F. Li, X. Wu, D. Xu, H. Zeng and L. Yuan, *Angew. Chem., Int. Ed.*, 2014, **53**, 11834–11839.
40 Q. Li, S. Lv, F. Xu, H. Deng, W. Zeng, J. Mao, Y.-X. Xu, S. Chen and L. Wang, *ACS Macro Lett.*, 2025, **14**, 1622–1630.
41 Z. Yang, K. Fu, W. Yu, A. Jia, X. Chen, Y. Cai, X. Li, W. Feng and L. Yuan, *Chin. Chem. Lett.*, 2025, **36**, 110842.
42 Z. Ye, M. Lian, Z. Yang, Y. Fu, Z. Wang, Y. Mu, S. Ji, H.-L. Zhang, L. Yuan, Z. Chi and Y. Huo, *Adv. Opt. Mater.*, 2023, **11**, 2202521.
43 X.-N. Xu, L. Wang and Z.-T. Li, *Chem. Commun.*, 2009, 6634–6636.
44 J. Zhu, X.-Z. Wang, Y.-Q. Chen, X.-K. Jiang, X.-Z. Chen and Z.-T. Li, *J. Org. Chem.*, 2004, **69**, 6221–6227.
45 P. F. Garrido, P. Rodríguez-Dafonte, L. García-Río and Á. Piñeiro, *Langmuir*, 2021, **37**, 11781–11792.

